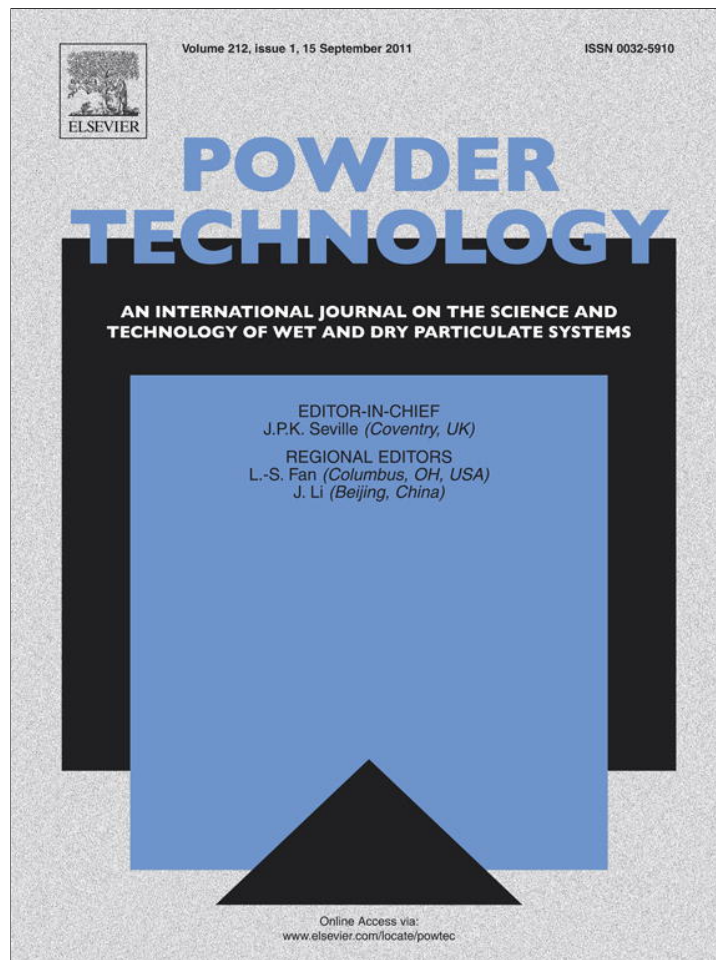


Provided for non-commercial research and education use.  
Not for reproduction, distribution or commercial use.



This article appeared in a journal published by Elsevier. The attached copy is furnished to the author for internal non-commercial research and education use, including for instruction at the authors institution and sharing with colleagues.

Other uses, including reproduction and distribution, or selling or licensing copies, or posting to personal, institutional or third party websites are prohibited.

In most cases authors are permitted to post their version of the article (e.g. in Word or Tex form) to their personal website or institutional repository. Authors requiring further information regarding Elsevier's archiving and manuscript policies are encouraged to visit:

<http://www.elsevier.com/copyright>



Contents lists available at ScienceDirect

Powder Technology

journal homepage: [www.elsevier.com/locate/powtec](http://www.elsevier.com/locate/powtec)

## Empirical analysis of eccentric flow registered by the DPIV technique inside a silo model

Irena Sielamowicz <sup>a,\*</sup>, Michał Czech <sup>b,1</sup>, Tomasz A. Kowalewski <sup>c,2</sup>

<sup>a</sup> 15-196 Białystok, Matejki 8, Poland

<sup>b</sup> Białystok Technical University, Mechanical Department, 15-351 Białystok, Wiejska 45 C, Poland

<sup>c</sup> Institute of Fundamental Technological Research, Polish Academy of Sciences, 00-049 Warsaw, Pawińskiego 5b, Poland

### ARTICLE INFO

#### Article history:

Received 24 September 2010

Received in revised form 5 April 2011

Accepted 20 April 2011

Available online 29 April 2011

#### Keywords:

Universal methodology of empirical analysis  
DPIV technique

Eccentric granular flow

Discharge on the left

Vertical model

Plexiglas

Velocity

Gaussian type function

Ch function

Multiple regression

"Joined functions"

Flow channel boundary (FCB)

### ABSTRACT

In this paper we continue empirical description of eccentric granular flow registered by the DPIV (Digital Particle Image Velocimetry) technique. The first results concerning eccentric flow with the outlet located on the right were published in Sielamowicz et al. [30]. Here we present a methodology of empirical descriptions of velocities, flow rate and the flow channel boundary (FCB) in another eccentric case. The analysis is based on the experimental results (velocity profiles) obtained in the DPIV technique. Statistical analysis of the experimental results was also performed. We show how to fit the proper type of function to describe flow parameters in the silo model. The presented methodology is universal and can be applied in any case of eccentric flow of any granular material.

© 2011 Elsevier B.V. All rights reserved.

### 1. Introduction

Investigation of eccentric filling and discharge in silos provides very interesting results and as it was stated in Sielamowicz et al. [30]. Results obtained in such analyses differ one from the other. In fact each experimental run is so specific that we can only identify the phenomena of eccentric behavior of the flowing material in silos. In practice eccentric processes occur very often and it may even lead to a disaster or damage of the structure. Changing the position of the filling pipe or the discharge outlet we can observe how the flowing material reacts to the structure. The task to identify flow patterns developed in the material during eccentric filling or discharge is still a challenge for engineers. Moreover to determine the flow rate, flow channel boundary (FCB) and wall stresses exerted by the flowing material seems to be much more valuable.

In this paper we present the methodology of empirical description of velocities, flow rate and stagnant zone boundary on the base of registered velocity fields in eccentric filling and discharge in 2D silo model. During asymmetrical flows, flow patterns formed in the silo and wall stresses exerted to the wall by flowing material may be quite different than in symmetrical case. That is why the problem to identify flow patterns developed in the material during eccentric filling or discharge, and to determine both the flow rate and wall stresses occurring under such state of loads is urgent to solve for engineers. The case of eccentric discharge was lately discussed by Sielamowicz et al. [30]. There are many measurements and experimental, theoretical analysis and predictions of the pattern of flowing material during discharge published by: Cundall and Strack [16], Nedderman and Tüzün [21], Tüzün and Nedderman [35], Haussler and Eibl [18], Runesson and Nilsson [27], Rotter et al. [25]. Predictions and investigations of eccentric flow patterns remain still a challenge for researchers.

### 2. Literature review

Silos are structures that are high, big with many tones of stored granular material or powder inside. The structure is calculated using

\* Corresponding author. Tel./fax: +48 85 6755997.

E-mail addresses: [irena.sielamowicz@gmail.com](mailto:irena.sielamowicz@gmail.com) (I. Sielamowicz), [mzech@pb.bialystok.pl](mailto:mzech@pb.bialystok.pl) (M. Czech), [tkowale@ippt.gov.pl](mailto:tkowale@ippt.gov.pl) (T.A. Kowalewski).

<sup>1</sup> Tel.: +48 85 7469307; fax: +48 85 7469559.

<sup>2</sup> Tel./fax: +48 22 826 98 03.

Standards where we can find fully calculating procedure but related to axial symmetric states of stresses. In Standard ENV 1991-4[3], the flow channel geometry and wall pressures under eccentric discharge are defined. Some Standards propose to increase the value coefficients of horizontal pressure during eccentric discharge (The Polish Standard PN-89/B-03262 [4], titled “Silosy żelbetowe na materiały sypkie. Obliczenia statyczne”). In other codes and guides as: ACI 313 [1], AS 3774 [2], Rotter [26] we can find eccentric discharge procedure but the approach is different in each of them. Jenike[19], Wood [39], Rotter [24] published theoretical solutions for the design of silos under eccentric discharge. The European Standard ENV 1991-4, [3] includes a comment on the eccentricity of the outlet, the definition of the flow channel geometry and wall pressure under eccentric discharge. One can find there the eccentric filling definition as a condition in which the top of the heap at the top of the stored solids at any stage of the filling process is not located on the vertical centerline of the silo. Also eccentric discharge definition is presented as a flow pattern in the stored solid arising from moving solid being asymmetrically distributed relative to the vertical centerline of the silo. This normally arises as a result of an eccentrically located outlet but can be caused by other asymmetrical phenomena which are not clearly defined. Calculations for flow channel geometry are required for only one size of flow channel contact with the wall for  $\Theta_c = 35^\circ$ . In Sielamowicz et al.[30] the wide discussion on methods of predicting flow channel dimensions and wall pressures under eccentric discharge is presented. Eccentric flows have also been investigated experimentally or numerically by Rotter [24,26], Ayuga et al. [6], Carson [9], Anon[5], Thompson et al. [33], Pokrant and Britton [22], Safarian and Harris[28], de Clercq[15], Blight [7], Borcz et al. [8], Shalouf and Kobiela[29], Molenda et al.[20], Chou et al. [13,14], Nedderman and Tüzün [21], Wójcik et al. [38]. FEM modeling in the analysis of influence of hopper eccentricity on wall pressures was presented by Guaita et al.[17] and Song and Teng[32]. One of the latest flow pattern measurements in a full scale silo was presented by Chen et al.[10]. One can find a long list of references concerning investigation of eccentric discharge there.

### 3. Experimental investigations

Choi et al.[11] and Chou et al.[12] also investigated velocities inside 2D bins. Our experiments were performed using transparent model of the silo made of acrylic glass. It has a form of a rectangular box with a height of 0.80 m, a depth of 0.10 m, and a width of 0.26 m, as shown in Fig. 1.

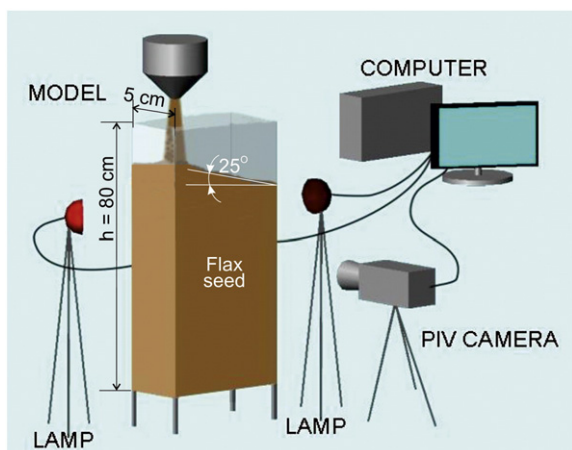


Fig. 1. Experimental setup.

The model was filled with flax seed supplied from the top through a feeding pipe. The bottom opening was used to collect granular material. To investigate the effects of eccentricity the model was filled from the left and the discharge opening was also located eccentrically on the left. The box was mounted on a metal frame with mechanisms to open the upper baffle used for feeding and the lower baffle used to release the granular material. Initially the upper baffle was left open for time necessary to fill the box with a given amount of grains. It was necessary to humidify the lab to assure that particles do not stick to the acrylic walls of the box due to static electricity. The clear side wall of the box was illuminated with several fluorescent lamps mounted along frames of the box. It allowed to obtain shadow free images of the seed. Additional tungsten lamp was mounted about 2 m from the box to improve contrast of the images.

The granular flow was observed in the vicinity of the transparent front wall of the model. For this purpose the flow of the seed was recorded by a high resolution CCD camera (PCO1200HS) with the objective 50 mm lens. Sequences of 12-bit images with the resolution of  $1280 \times 1024$  pixels were acquired by Pentium 4 based personal computer using IEEE1394 interface. Long sequences of images taken at properly defined time intervals were taken during the whole period of the box feeding and discharging process. These images were used to characterize the flow of the granular material.

In many aspects, the flow of granular material resembles flow of fluid suspension. Hence, fluid mechanical approach based on the Particle Image Velocimetry (PIV) technique can be applied to evaluate instantaneous displacements of the seed particles. The Particle Image Velocimetry is an optical method of fluid visualization used to obtain instantaneous velocity field measurements. The fluid is seeded with tracer particles which, for the purposes of PIV, are generally assumed to faithfully follow the flow dynamics. It is the motion of these seeding particles that is used to calculate velocity information of the flow being studied. For this purpose the frames of images are split into a large number of interrogation areas, or windows. It is then possible to calculate a displacement vector for each window with the help of signal processing and autocorrelation or cross-correlation techniques. This is converted to a velocity using the time between image shots and the physical size of each pixel on the camera. During PIV measurement in fluids, the particle concentration is such that it is possible to identify individual particles in an image, but not with certainty to track it between images.

When the particle concentration is too high, as in the case of granular material, it becomes impossible to obtain correct evaluation of images with the help of classical image correlation techniques. Hence, here we proposed to replace the classical PIV image evaluation with an extended version of the Optical Flow DPIV image analysis [23]. Sequences of ordered images were used for the estimation of motion as discrete image displacements using the Optical Flow method to calculate the displacement of pixels between two image frames which are taken at the given time interval. Optical flow or optic flow is the pattern of apparent motion of objects, surfaces, and edges in a visual scene caused by the relative motion between an observer (an eye or a camera) and the scene, and can be used for any optical objects with no homogeneous surface texture. In case of the seed flow images this condition is attained as each grain has little difference in optical appearance and can be identified on the frame as intensity variation. The technique that we choose for the DPIV application is based on the Orthogonal Dynamic Programming (ODP) algorithm for optical flow detection from a sequence of images. It performs a global image match by enforcing continuity and regularity constraints on the flow field. This helps in ambiguous or low particle density regions. It provides dense velocity fields (neither holes nor border offsets) and greatly improves the accuracy in regions with strong velocity gradients. The algorithm used is based on the search of a transformation that relates the second image to the first one and minimizes the optical differences between

them. The matching is global and does not require any previous segmentation or feature extraction. The main idea is to transform the search problem for two dimensional displacements into a carefully selected sequence of search problems for one-dimensional displacements, thereby decreasing greatly the complexity. First, the two images are identically sliced into several parallel overlapping strips. Then, for every pair of strips, an optimal match is searched for with displacements allowed only in the slicing direction and identical for all the pixels in the same column in the orthogonal (here horizontal) direction. A dense field of displacements (between column vectors) is found for every pair of strips minimizing the optical intensity differences between them with the help of a dynamic programming algorithm. This gives us a displacement value at every point of all strips. Then, displacement values for all other pixels of the image are interpolated (or extrapolated) from the pixel values of the nearest strips. A dense displacement field is obtained for the whole image. This displacement field is then smoothed before the following steps of the algorithm are applied.

The method was successfully tested as a supplement of the classical Particle Image Velocimetry (PIV), commonly used in fluid mechanics to extract velocity fields of seeded flow. It was found that two (in-plane) components of the velocity vectors can be recovered using a single camera within the 4–8% range of errors if two images are used [23]. Increasing number of images in the evaluated sequence improves evaluation accuracy on cost of computational time. In the following the displacement (velocity) field was evaluated using triplets of images. The Optical Flow DPIV technique allowed us to obtain dense velocity fields with displacement vectors found for each pixel of the image. This information is used for further evaluation of the velocity profiles, velocity contours and streamlines. Here, the term “streamline” is defined as a virtual path of a seed particle evaluated from the calculated instantaneous velocity field. Calibration carried out for synthetic sequences of images shows that the accuracy of measured displacement is about 0.5 pixel/frame for tested two-image sequences and 0.2 pixel/frame for four-image sequences.

In this paper we apply the Optical Flow technique DPIV to investigate dynamic behavior of granular material during discharge and measure flow profiles, velocity distributions, vector fields in plane flow hoppers with eccentric filling and discharge. In order to evaluate velocity long sequences of 100–400 images were taken at variable

time intervals covering the whole discharge time. Velocity profiles obtained that way for the flow of granular material inside a quasi-two-bottomed silo were smooth and free of shock-like discontinuities. So produced velocity field was used to obtain natural track of individual particles by integrating virtual paths of selected points of the evaluated velocity field.

#### 4. Theoretical description of velocities

We present the methodology of theoretical analysis of velocities in asymmetric flow of flax seed in the model with vertical and smooth walls with outlet located close to the left wall. We consider the case discussed in Fig. 2 where the flow mode is also presented. The model has the depth of 5 cm. Properties of the granular material used in the experiment: angle of wall friction against Plexiglas  $\varphi_w = 26^\circ$ , angle of internal friction  $\varphi_e = 25^\circ$ , Young modulus  $E = 6.11$  MPa, granular material density deposited through a pipe with zero free-fall  $\rho_b = 746$  kg/m<sup>3</sup> at 1 kPa and 747 kg/m<sup>3</sup> at 8 kPa. Fig. 2 presents velocity contours and Fig. 3 velocity profiles that were used to statistical analysis. The readings taken from velocity profiles (cf. Fig. 3) are given in Tables 1–7 in Appendix A. As it is seen in Fig. 3 the part of the storage material has a value equal to zero for the vertical velocity. This happens in the stagnant zone that is indicated with blue color in Fig. 2. Values equal to zero for the vertical velocity are presented by the velocity profiles in Fig. 3 where the profiles coincide with each other in the range of the stagnant zone.

Statistical analysis of the experimental results was done applying the values given in Tables 1–7 (given in Appendix A). The confidence intervals were determined for the analyzed levels for the averages of analyzed velocities, [37] and listed in Tables 8–13 in Appendix A. It was considered that the speed does not vary with time of discharge as accepted of the level of confidence of 95%. In this analysis there are no readings that were removed from the data set. Velocity distributions at analyzed levels ( $H = 5, 10, 20, 30, 40$  and  $50$  cm) (Fig. 4) are made on the basis of the values of average velocities given in Tables 8–13 in Appendix A. For level  $H = 60$  cm velocity distribution was made using the experimental readings listed in Table 7 in Appendix A.

On the basis of velocity profiles presented in Fig. 3 and the data listed in Tables 1–7 (Appendix A), an inconsiderable dependence of the velocity on time and on the height of the measurement points has been found, especially for the instant  $t = 1$  s and the height  $H = 5$  cm

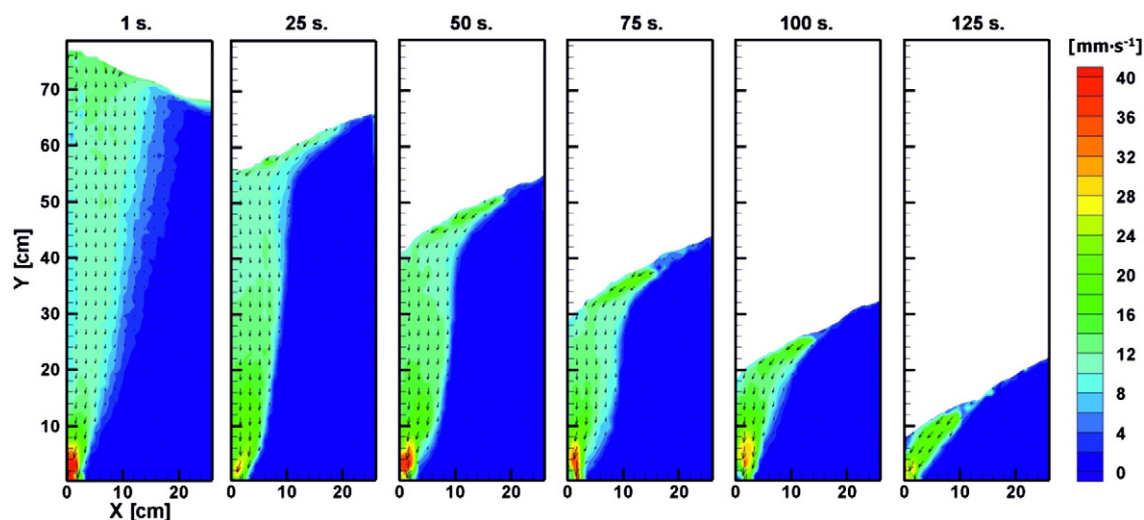


Fig. 2. Velocity distributions in the flowing flax seed in the model.

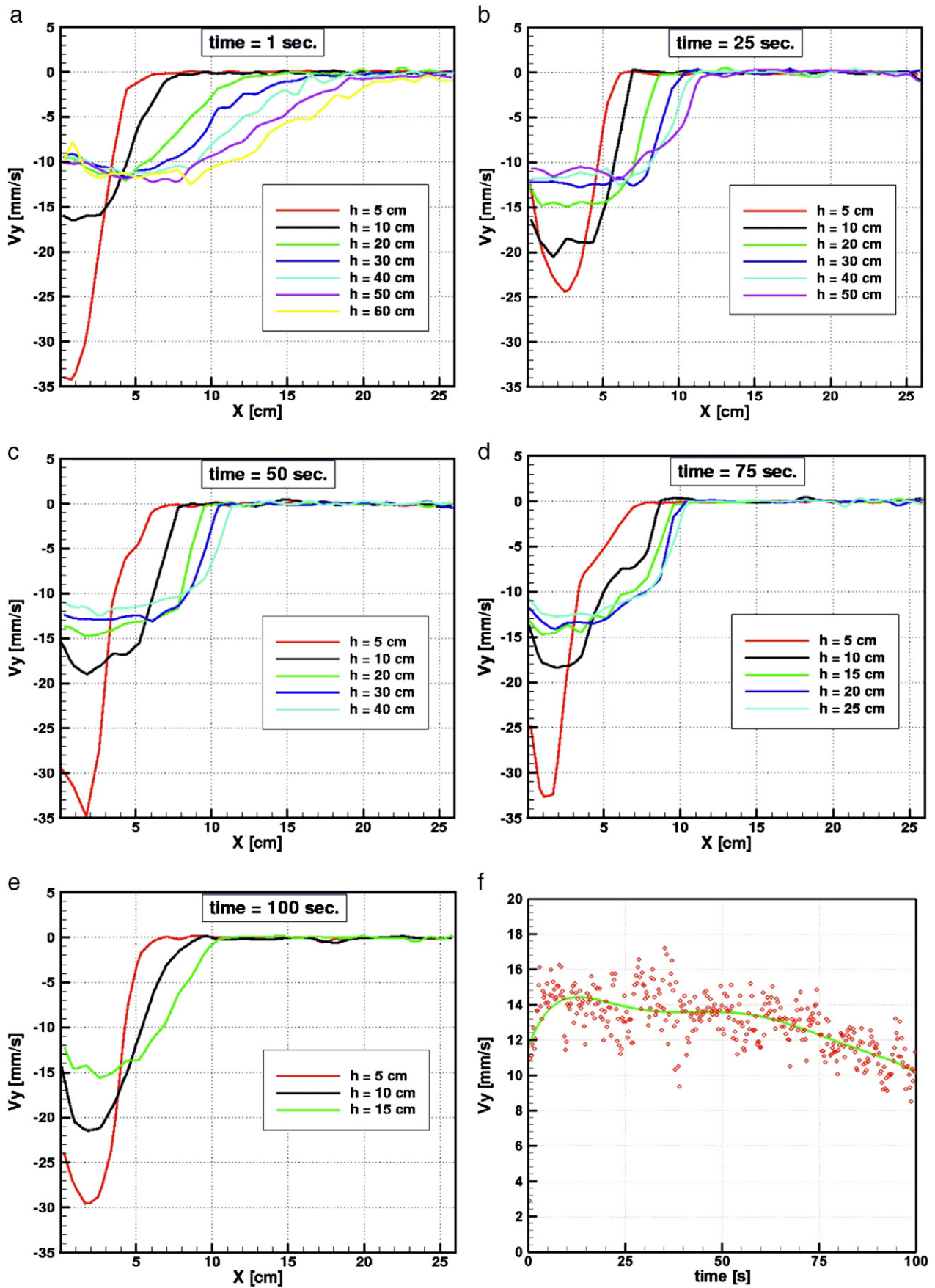


Fig. 3. a–e) Velocity profiles of flax seed at various time instants, f) velocity distribution in time; g–i) velocity distribution on the analyzed levels.

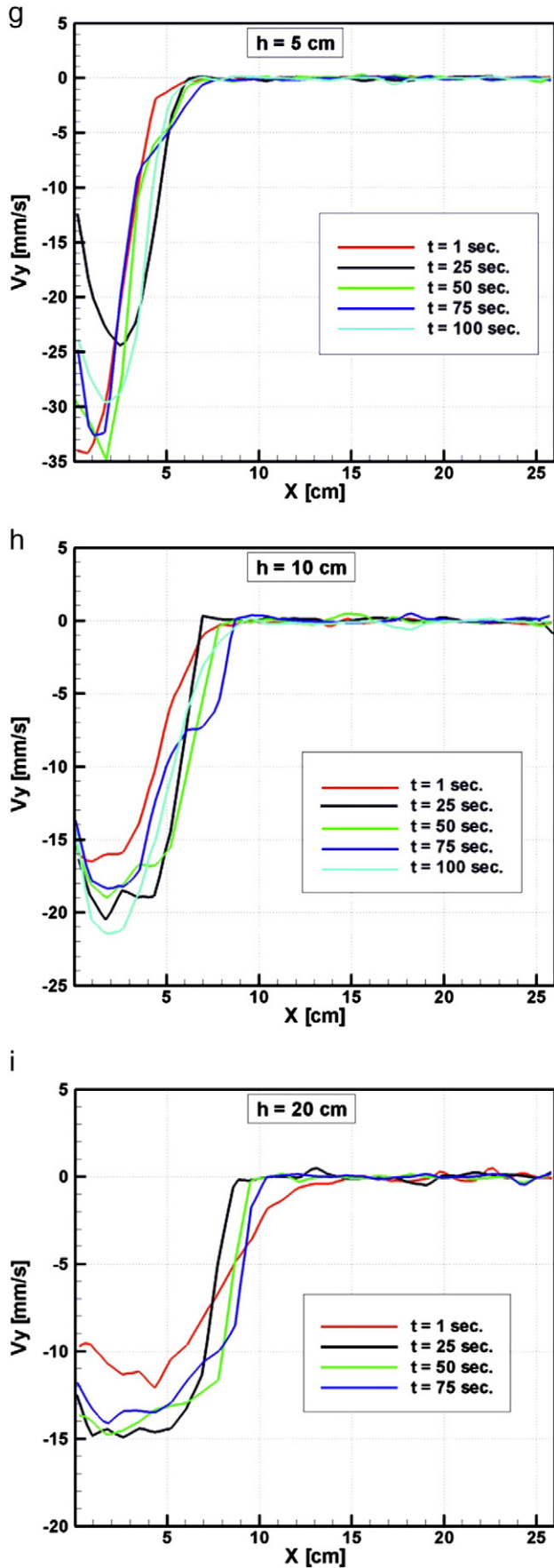


Fig. 3 (continued).

above the bottom of the model. In the further analysis the average values of velocities calculated both for the given levels and for the distances from the symmetry axis have been applied. The data presented in Tables 8–13 confirmed the independence of the analyzed velocities on time. In fact we can find the measurement points, located i.e. at  $x = 7$  cm and  $x = 8$  cm and levels  $H = 30, 40$  and  $50$  cm where velocities are similar and they can be described by one curve or the parameters of the curves should be similar.

4.1. Description of velocities by the exponential function (modified, the Gaussian type)

In the analysis presented below we depend vertical velocity component  $V_y$  on the distance  $x$  and on location of various heights  $z$  (or levels marked with  $H$ ). Empirical description of vertical velocity  $V_y$  calculated in the units of millimeters per second was proposed according to the function:

$$V_y = Ae^{Bx + Cx^2} \tag{1}$$

where parameters  $A, B$  and  $C$  were determined by the least squares method (the first regression) and listed in Table 1. Formula (1) in Sielamowicz et al. [30] is of the same type as in this paper though in Sielamowicz et al. [30] the model had the other location of the outlet. Parameters in both Formulas are described by other type of function depending on the height. In Sielamowicz et al. [30] it is parabola (Formula 2), and in this paper we applied hyperbola (Formula 2) that has an influence to the quantity and the form of terms in Formula 3 in both articles. Applying such description (parabola in Sielamowicz et al. [30] contra hyperbola used in this paper) Formula 3 has a quite different form and quantity of terms. Similar situation is applied in description of velocities by  $ch$  function in both papers.

Distributions of parameters  $A, B$  and  $C$  after the 1st regression are shown in Fig. 5. The points denote the values of the parameters and the solid lines the empirical description of the parameters at various analyzed levels.

In the further analysis, parameters  $A, B$  and  $C$  were depended on the height  $z$  in the model in the following form:

$$\begin{aligned} \hat{A} &= A_0 + A_1 / z \\ \hat{B} &= B_0 + B_1 / z \\ \hat{C} &= C_0 + C_1 / z \end{aligned} \tag{2}$$

and their values  $A_i, B_i, C_i$  for  $i = 0, 1$  were determined by the least squares method (the 2nd regression) and listed in Table 2.

Velocity distributions were made on the basis of Formulas (1), (2) and values listed in Table 2. Fig. 6 presents the average experimental results  $\bar{V}_y \text{ exp}$  and the empirical values  $\hat{V}_y \text{ empir}$  after the 1st regression (after depending the velocity on the distance from the symmetry axis  $x$ ) and after the 2nd regression  $\hat{V}_y \text{ empir}$ , (depending the velocity both on the distance  $x$  and on the height  $z$ ).

On the basis of the 1st and the 2nd regression the description of vertical velocity was assumed in the form of the following function:

$$V_y = \exp(a_0 + a_1x_1 + a_2x_2 + a_3x_3 + a_4x_4 + a_5x_5) \tag{3}$$

where:  $x_1 = \frac{1}{z}, x_2 = x, x_3 = \frac{x}{z}, x_4 = x^2, x_5 = \frac{x^2}{z}$ , and  $x$  denotes the distance from the left wall,  $z$  – is the due height in the model, measured in centimeters.

Coefficients  $a_i$  where  $i = 0, 1 \dots 5$  were calculated using the least squares method, and listed in Table 3. We define the calculations accurately using the multiple regression. There is a possibility to determine the parameters in Formula (3) by the nonlinear regression, that would define the description a little more accurately.

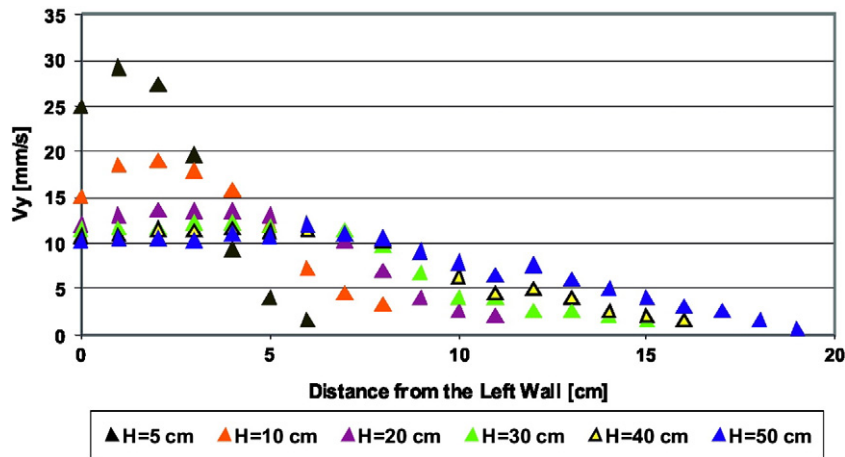


Fig. 4. Average velocities at various analyzed levels in the model.

On the basis of Formula (3) and data listed in Table 3, the values of vertical velocity  $\hat{V}_y$  were calculated using the multiple regression. Three approaches of describing velocity in the model presented above are shown in Fig. 6. The points denote average values of experimental measurements and the solid lines represent the functional descriptions of velocity after the 1st ( $\hat{V}_y$ ), the 2nd ( $\hat{V}_y$ ) and the multiple regression ( $\hat{V}_y$ ).

4.2. Description of velocities by ch function

In our analysis we search the best description of velocities that were measured during experiments. Another description of velocity was proposed by the ch function in the following form:

$$V_y = ch(A + Bx + Cx^2). \tag{4}$$

Using the 1st regression the velocity depended on the distance  $x$ . The parameters  $A$ ,  $B$  and  $C$  were calculated by the least squares method and listed in Table 4.

Using the 2nd regression according to Formula (2) the velocity depended both on the distance  $x$  measured from the left wall and on the height  $z$ . Parameters  $A_i$ ,  $B_i$  and  $C_i$  were calculated by the least squares method and given in Table 5.

On the basis of the 1st and 2nd regression we assumed the description of vertical velocity as a following function:

$$V_y = ch(a_0 + a_1x_1 + a_2x_2 + a_3x_3 + a_4x_4 + a_5x_5). \tag{5}$$

Table 1  
Values of the symbols given in Formula (1), (1st regression).

Level H [cm]	A	B	C
5	25.381	0.2623	-0.1239
10	15.69	0.1873	-0.04985
20	11.078	0.1943	-0.03269
30	11.577	0.06821	-0.01433
40	10.157	0.09630	-0.01359
50	9.412	0.09173	-0.01022
60	8.719	0.1087	-0.009013

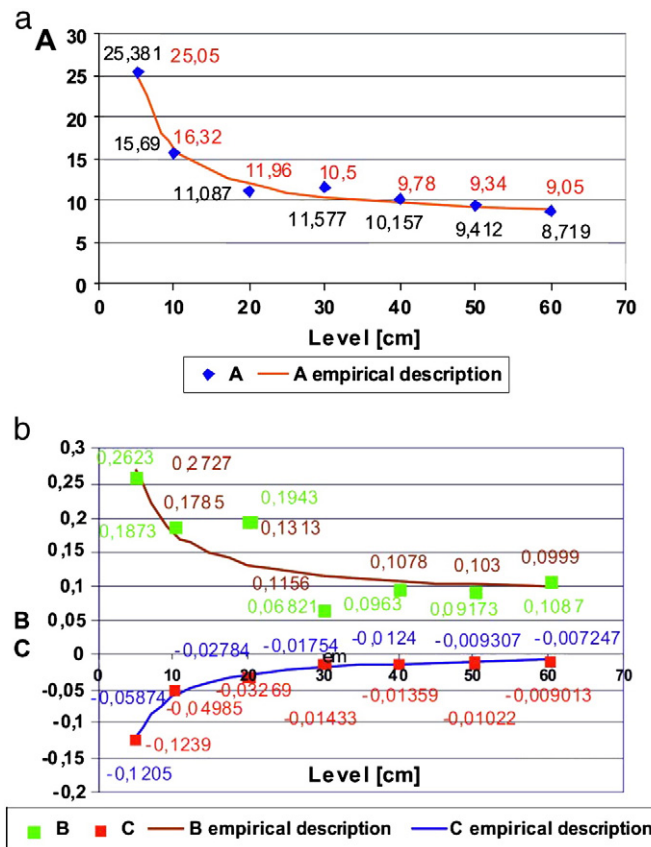


Fig. 5. Distributions of parameters A, B and C (points) and their empirical descriptions (solid lines).

Table 2  
Values of the symbols given in Formula (2), (2nd regression).

Parameters	$i=0$	$i=1$	R coefficient of correlation
$A_i$	7.596	87.267	0.9934
$B_i$	0.08419	0.9427	0.8823
$C_i$	0.003051	-0.61786	-0.9937

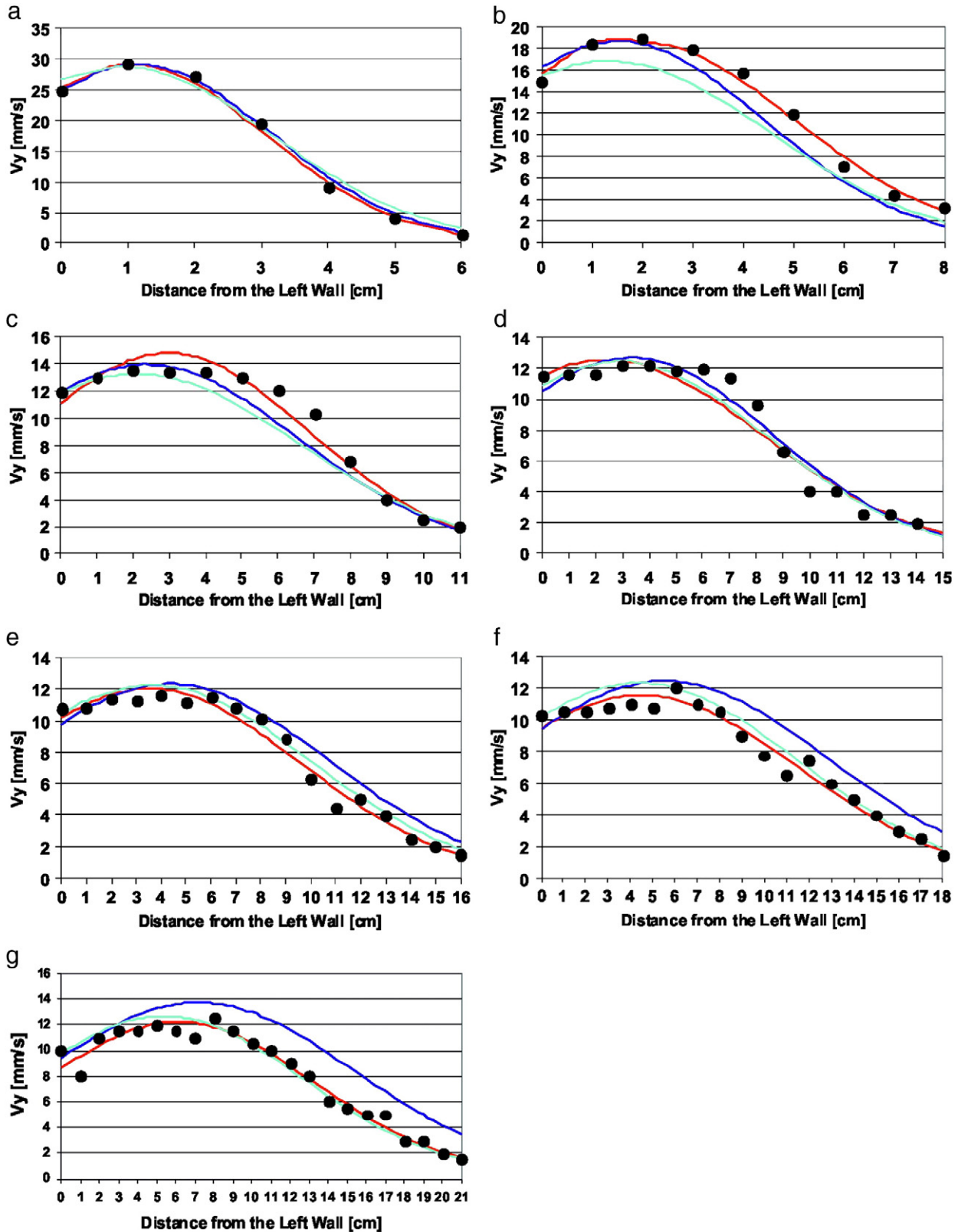


Fig. 6. Velocity distributions: average experimental results compared with the 1st, the 2nd and the multiple regression.

The values of parameters  $a_i$  (where  $i=0,1...5$ ) were calculated using the least squares method and listed in Table 6. Variables  $x_1, x_2, x_3, x_4,$  and  $x_5$  are applied like in Formula (3).

Applying three regressions we present both the empirical description of vertical velocity by the  $ch$  function and distributions of vertical velocity in Fig. 7.

**Table 3**  
Values of coefficients  $a_i$  in Formula (3).

$a_0$	$a_1$	$a_2$	$a_3$	$a_4$	$a_5$
2.2055	5.3965	0.0799	0.4510	-0.000585	-0.4743

4.3. Description by “the joined functions of generalized Gaussian type”

Analyzing the results of the description of velocities in the previous section especially the 1st regression presented in Figs. 6 and 7, we notice that good agreement to the average experimental results is given both by the function of the Gaussian type as well as by the  $ch$  function. Because of the specific nature of the flow in the asymmetric configuration we discuss here another description of velocities by functions of the same type but with various parameters in two different regions. One part of the velocity profile curve is described by one function and the other part by another function. In the analysis we divide the set  $x$  into two subsets: the first with  $x \in \langle 0, x_{\frac{n}{2}} \rangle$  for even points, and  $x \in \langle 0, x_{\frac{n+1}{2}} \rangle$  for odd points and the second subset with  $x \in \langle x_{\frac{n}{2}}, x_n \rangle$  for even points and  $x \in \langle x_{\frac{n+1}{2}}, x_n \rangle$  for odd points. Figs. 8 and 9 present the area limited by any velocity profile and the coordinate system with functions ascribed to the due parts of the curves.

The first part of the velocity profile is described by the following function:

$$\hat{V}_{y_1} = y_1 = A_1 e^{B_1 x + C_1 x^2} \quad (6)$$

and the second part of the curve by the function:

$$\hat{V}_{y_2} = y_2 = A_2 e^{B_2 \left(x - x_{\frac{n}{2}}\right) + C_2 \left(x - x_{\frac{n}{2}}\right)^2} \quad (7)$$

if the number of measurement points  $n$  is even. In the case if the number of measurement points is odd then the velocity profile is described by function (8) and the following function in the due parts:

$$\hat{V}_{y_2} = y_2 = A_2 e^{B_2 \left(x - x_{\frac{n+1}{2}}\right) + C_2 \left(x - x_{\frac{n+1}{2}}\right)^2} \quad (8)$$

where  $A_2 = \hat{y}_1 \left(x_{\frac{n}{2}}\right)$  for even points and  $A_2 = \hat{y}_1 \left(x_{\frac{n+1}{2}}\right)$  for odd points. Parameters  $A_1, B_1, C_1$  and  $B_2, C_2$  were determined by the least squares method. In Fig. 10 the descriptions of vertical velocity by “the joined functions” are presented.

Comparing the experimental velocity values to the description made by the first regression we can notice that the convergence of the obtained results is good in both intervals of the analysis.

**Table 4**  
Parameters  $A, B$  and  $C$  from Formula (4), the 1st regression.

Level H [cm]	A	B	C
5	3.914	0.2935	-0.1318
10	3.443	0.1913	-0.05063
20	3.088	0.2028	-0.03386
30	3.127	0.07823	-0.01538
40	2.994	0.1055	-0.01437
50	2.918	0.09999	-0.01086
60	2.841	0.1159	-0.009498

**Table 5**  
Values of the symbols given in Formula (2), (2nd regression).

Parameters	$i=0$	$i=1$	R coefficient of correlation
$A_i$	2.838	5.524	0.9853
$B_i$	0.08839	1.0528	0.9094
$C_i$	3.5562	-0.6546	-0.992

4.4. Comparison of empirical descriptions of velocities

4.4.1. Comparison of empirical descriptions of velocities using the Gaussian and the  $ch$  function

Verification of accuracy of the applied descriptions was made by calculating the sums of the squares of the differences of velocities in three applied regressions by the Gaussian description and by the  $ch$  function. The values are listed in Table 7.

The 1st and the multiple regression in both descriptions of velocities (by the function of the Gaussian type and by the  $ch$  function) provide the similar results that indicate the right choice of the functions. The 2nd regression gives a better agreement to the experimental results by the Gaussian description, but the regression was only applied to determine the type of the function. In fact, we search the multiple regression. If we calculated the 1st and the multiple regression we would see that both descriptions of velocities are almost similar. This fact can be analyzed in Figs. 6 and 7 comparing the proper curves.

4.4.2. Comparison of velocities using the Gaussian description in the whole interval of the flow using the Gaussian and the “joined function”

Accuracy of the applied method was investigated by calculating the sums of the squares of differences of velocities. The results from Table 8 can be compared with data given in Table 7. The description made by “the joined functions” gives the least sum of the squares of the differences of velocities. But we can state that in such specific flow there are no methods to describe velocities in an accurate way both at all analyzed levels and at all measurement points. Thus if the description of velocities is due at lower levels then it does not describe velocities accurate at higher levels. And vice versa.

The description of velocities was made using the Gaussian and the “joined functions.” The better accuracy was obtained using the “joined functions” because the value of the sums of the squares of the differences of velocities was 21.96 comparing to 49.88 obtained using the generalized Gaussian description, (cf. Fig. 11).

4.5. Empirical description of flow rate

The flow rate  $Q$  was calculated for three presented descriptions of velocities.

4.5.1. Empirical description using the Gaussian function

In the solution given by the Gaussian exponential function, the flow rate was calculated according to the following formula:

$$Q = \int_0^{x_{\max}} A e^{Bx + Cx^2} dx \quad (9)$$

**Table 6**  
Values of coefficients  $a_i$  in Formula (5).

$a_0$	$a_1$	$a_2$	$a_3$	$a_4$	$a_5$
2.8743	5.5093	0.0903	0.4736	-0.000817	-0.4980

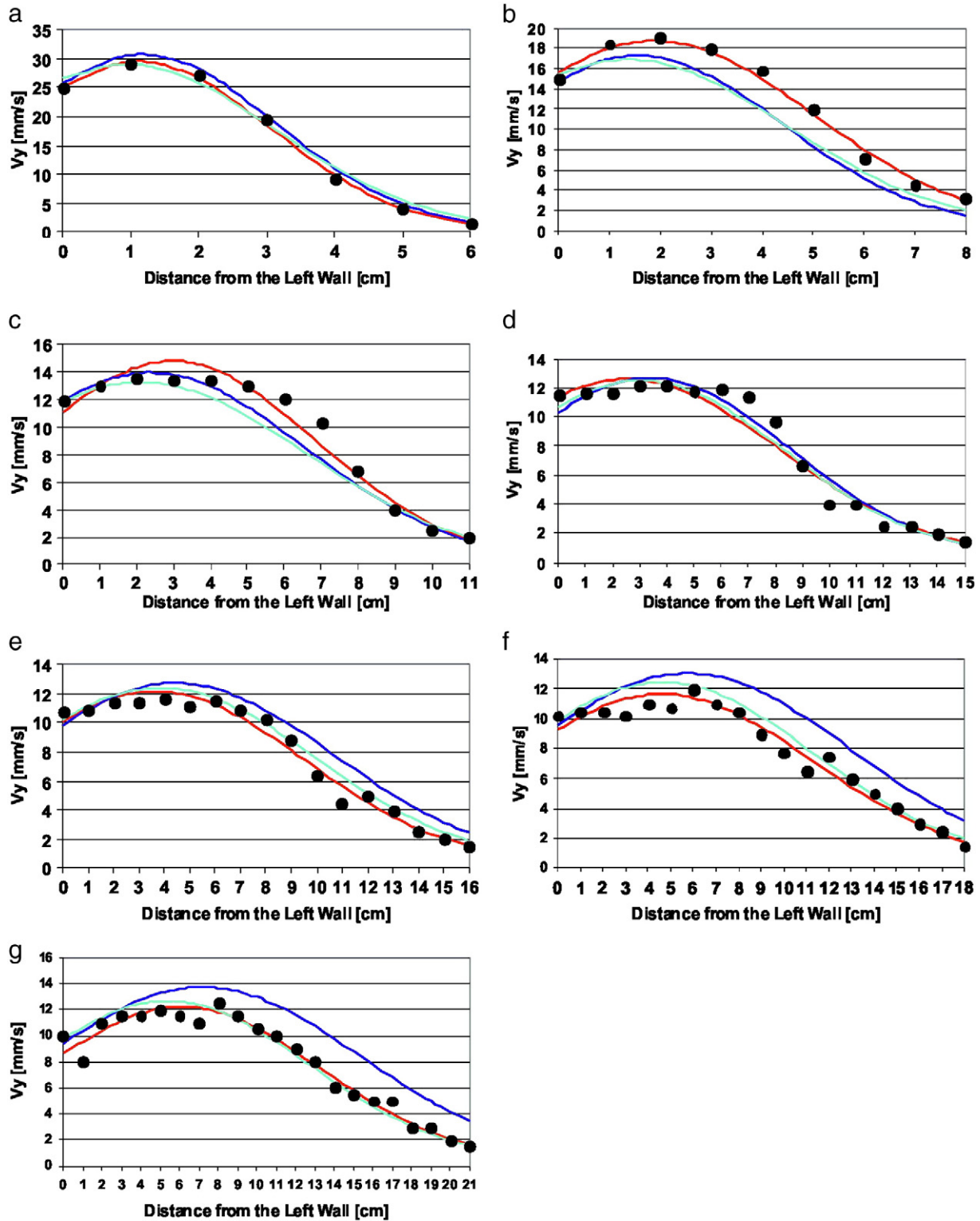


Fig. 7. Vertical velocity descriptions by the three applied methods.

and the values are listed in Table 9. Parameters from Formula (9) were taken from Table 1. In Formula (9) and (11) the limit of integration  $x_n$  denotes the number and position of the last measurement point calculated from the left wall taken from the experimental readings for

various analyzed levels, (cf. Tables 1–7 in Appendix A). The flow rate was described by the following parabolic function:

$$\tilde{Q} = \tilde{A}_1 + \tilde{B}_1 z + \tilde{C}_1 z^2 \quad (10)$$

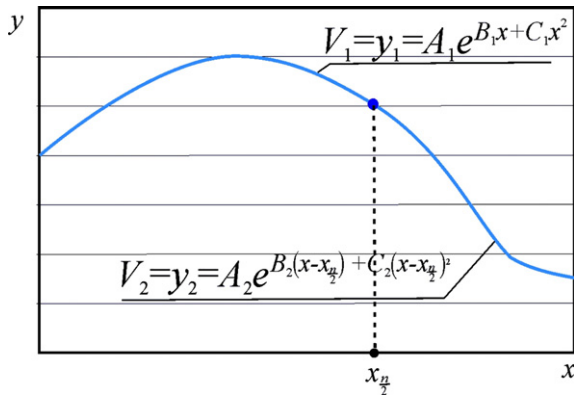


Fig. 8. Velocity profile and its description by two functions, for even points.

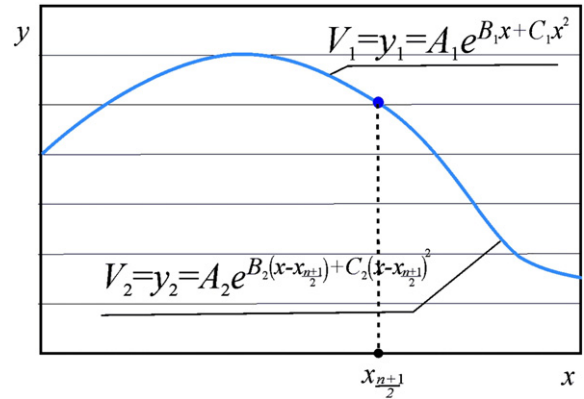


Fig. 9. Velocity profile and its description by two functions, for odd points.

where parameters  $\tilde{A}_1 = 104.03$ ,  $\tilde{B}_1 = -0.2808$ ,  $\tilde{C}_1 = 0.0233$  were calculated by the least squares method using the values listed in Table 9. Using parameters  $\tilde{A}_1$ ,  $\tilde{B}_1$ ,  $\tilde{C}_1$ , the values of the flow rate  $\tilde{Q}$  were determined and these values were used to calculate the sums of the squares of the differences of the flow rate that are listed in Table 9.

#### 4.5.2. Empirical description using the *ch* function

In the description of velocities by the *ch* function, the flow rate was obtained by calculating the following integral:

$$Q = \int_0^{x_n} ch(A + Bx + Cx^2) dx \quad (11)$$

and the values listed in Table 9. Parameters  $A$ ,  $B$  and  $C$  in Formula (11) were taken from Table 4. The limit of integration  $x_n$  was used like in Formula (9). The flow rate  $\tilde{Q}$  was also described by the parabolic function:

$$\tilde{Q} = \tilde{A}_2 + \tilde{B}_2 z + \tilde{C}_2 z^2 \quad (12)$$

where parameters  $\tilde{A}_2 = 104.39$ ,  $\tilde{B}_2 = -0.2902$ ,  $\tilde{C}_2 = 0.02346$  were determined by the least squares method using the values listed in Table 9. Using parameters  $\tilde{A}_2$ ,  $\tilde{B}_2$ ,  $\tilde{C}_2$ , the values of the flow rate  $\tilde{Q}$  were calculated and used to determine the sums of the squares of the differences of the flow rate that are also listed in Table 9.

#### 4.5.3. Flow rate calculated by using the “joined functions” of generalized Gaussian type

In the description of velocities the flow rate  $Q$  was calculated as integrals both for even and for odd points:

– for even points:

$$Q = \int_0^{x_{n/2}} \hat{V}_{y_1} dx + \int_{x_{n/2}}^{x_n} \hat{V}_{y_2} dx \quad (13)$$

– and for odd points

$$Q = \int_0^{x_{(n+1)/2}} \hat{V}_{y_1} dx + \int_{x_{(n+1)/2}}^{x_n} \hat{V}_{y_2} dx \quad (14)$$

where:  $n$  denotes the abscissa  $x$  at which the given functions join to each other and  $x_n$  is the last measurement point for velocity profiles.

#### 4.5.4. Comparison of description of the flow rate values calculated using three methods

In three cases the calculated values of the flow rate  $Q$  [cm<sup>2</sup>/s] are almost similar, both in the empiric description by the parabolic function and as integrated values.

Fig. 12 presents variation of the flow rate calculated by the function of the Gaussian type (a) and by the *ch* function.

It is noticeable that in the region between level  $H = 5$  cm and level  $H = 10$  cm the increase of the flow rate reaches approximately the similar values. From level  $H = 20$  cm up the increase of the flow rate is not constant. As a result of differentiating Formula (9) we obtain the linear relation of the increment of velocity of the flow rate at different levels. The difference of the flow rate reaches 0.939 [cm<sup>2</sup>/s] between levels  $H = 20$  cm and  $H = 30$  cm and 0.928 [cm<sup>2</sup>/s] between levels  $H = 30$  cm and  $H = 40$  cm, respectively. But higher than  $H = 40$  cm the flow rate increases rapidly because the flow channel widens and more material flows into it. The increase between level  $H = 40$  cm and  $H = 50$  cm is already 1.621 [cm<sup>2</sup>/s] and between level  $H = 50$  cm and  $H = 60$  cm reaches 2.916 [cm<sup>2</sup>/s]. Here we analyzed the integrated values in the description by the Gaussian function. The similar situation occurs in the calculations of the flow rate in the description by the *ch* function.

The flow rate was described by the parabolic function according to Formulas (13) or (12). Parameters  $\tilde{A} = 105.12$ ,  $\tilde{B} = -0.3033$  and  $\tilde{C} = 0.02303$  were calculated by the least squares method. The values of the flow rate  $Q$  [cm<sup>2</sup>/s] are listed in Table 9. Fig. 13 presents the graphical distribution of the flow rate. It is noticeable that in the region between level  $H = 5$  cm and  $H = 10$  cm again the flow rate increment is 0.192 [cm<sup>2</sup>/s] and between  $H = 10$  cm and  $H = 20$  cm already reaches 0.499 [cm<sup>2</sup>/s], respectively. From level  $H = 20$  cm and higher the increase of the flow rate is not constant and increases rapidly. The difference of the flow rate reaches 1.057 [cm<sup>2</sup>/s] between levels  $H = 20$  cm and  $H = 30$  cm and 0.803 [cm<sup>2</sup>/s] between levels  $H = 30$  cm and  $H = 40$  cm, respectively. But higher than  $H = 40$  cm the flow rate increases rapidly. The increase between level  $H = 40$  cm and  $H = 50$  cm is already 1.435 [cm<sup>2</sup>/s] and between level  $H = 50$  cm and  $H = 60$  cm reaches 3.049 [cm<sup>2</sup>/s], respectively.

The values of the flow rate calculated by the “joined functions” approximate the values calculated by the Gaussian description and the *ch* function. As a conclusion of the analysis we can state that there are levels at which more accurate descriptions have been found and levels with not so good descriptions. Generally all the applied methods provide almost the same description.

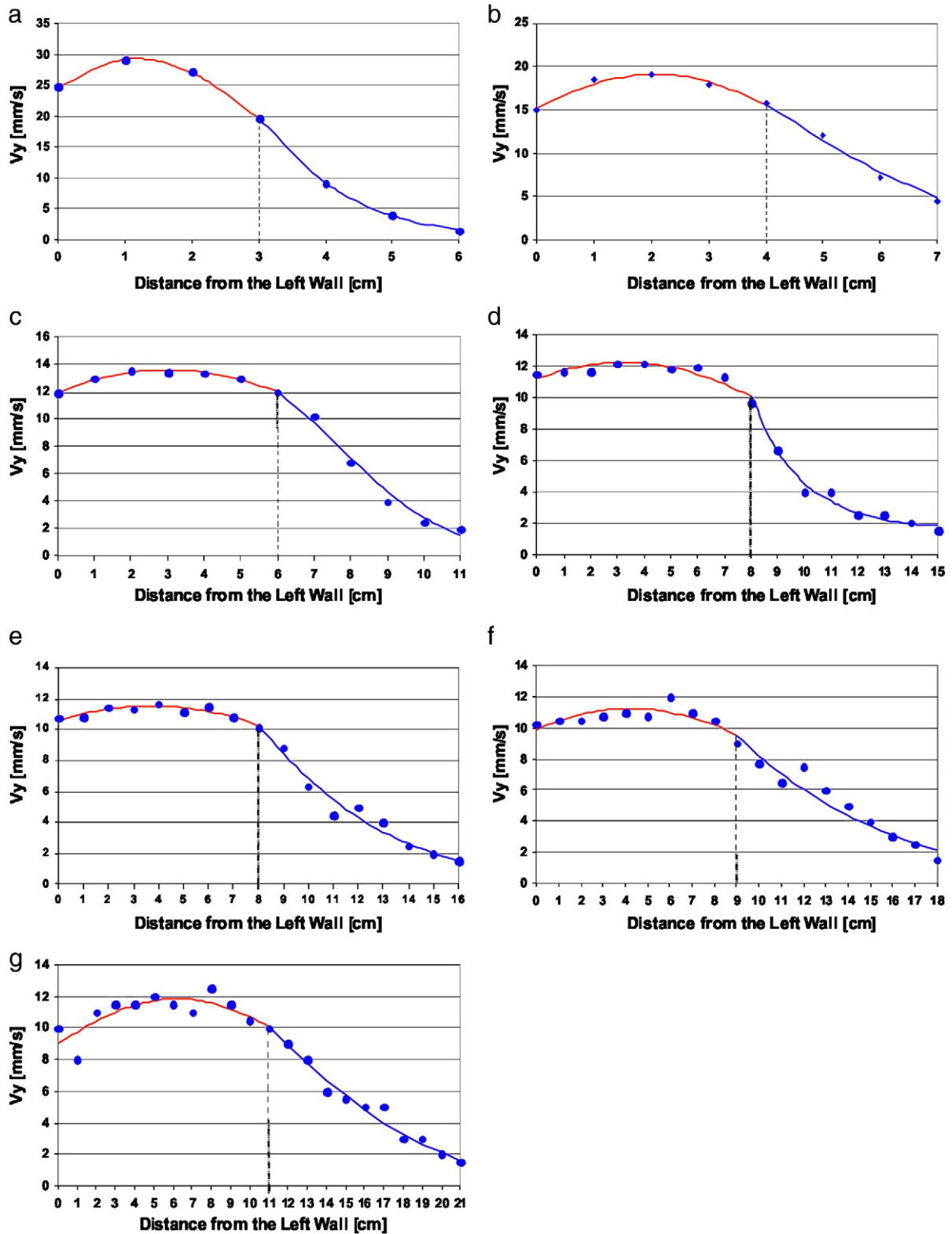


Fig. 10. Vertical velocity descriptions by the “joined functions”.

#### 4.6. Empirical determination of the channel flow boundary (CFB)

Using the readings from Tables 1–7 given in Appendix A, the distances  $x_i$  (for instance  $x = 2, 3, 4, 5$  cm) were determined from the left wall of the model. The last four readings of velocities  $V_y$  of nonzero

values were taken for the analysis. Velocities  $V_y$  depended on  $x$  by the functions of: the parabolic type  $\hat{V}_y = A + Bx + Cx^2$ , hyperbolic type  $\hat{V}_y = A + \frac{B}{x}$ , or linear type  $\hat{V}_y = a + bx$ . We searched the values  $x$  at which  $V_y = 0$  (flow channel boundary). At first we applied the

**Table 7**  
Sums of the squares of the differences of velocities.

Regression	Sums of the squares of the differences of velocities measured at the analyzed levels $\sum (V_{yemp} - \bar{V}_{yexp})^2$							$\sum \sum (V_{yemp} - \bar{V}_{yexp})^2$
	5 cm	10 cm	20 cm	30 cm	40 cm	50 cm	60 cm	
<i>Gaussian description</i>								
1st	4.128	2.790	8.132	14.195	5.423	6.250	8.962	49.88
2nd	4.002	26.504	16.378	10.058	20.533	40.901	50.936	169.31
Multiple	16.001	49.529	24.520	11.554	7.969	12.557	15.311	137.44
$\sum \sum$	24.131	78.823	49.030	35.807	33.925	59.708	75.209	356.63
<i>Description by the ch function</i>								
1st	2.431	2.737	8.843	12.875	5.503	6.780	9.280	48.45
2nd	8.717	51.069	24.526	9.920	28.413	72.162	108.568	303.37
Multiple	13.218	50.413	24.037	10.691	8.857	15.478	15.303	138.00
$\sum \sum$	24.366	104.219	57.406	33.486	42.773	94.420	133.151	489.82

**Table 8**  
Sums of the squares of the differences of velocities.

Description method	Sums of the squares of the differences of velocities measured at the analyzed levels $\sum (V_{yemp} - \bar{V}_{yexp})^2$							$\sum \sum (V_{yemp} - \bar{V}_{yexp})^2$
	5 cm	10 cm	20 cm	30 cm	40 cm	50 cm	60 cm	
"Joined functions"	0.0117	1.3702	1.2453	1.8206	2.4789	6.6774	8.3527	21.96

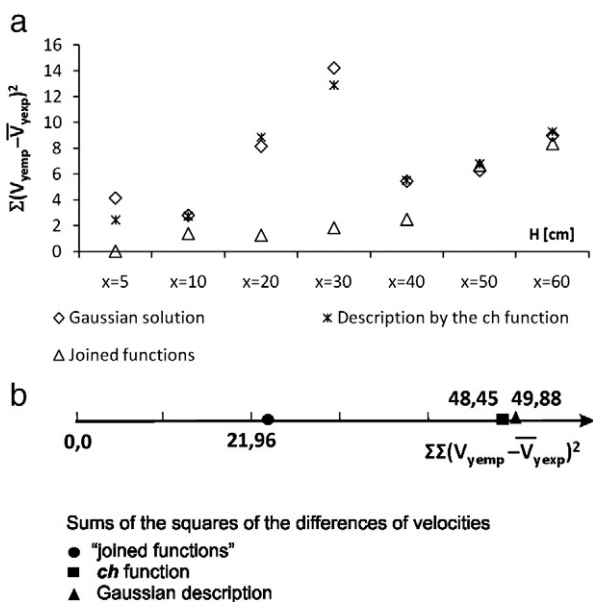


**Fig. 11.** Comparative analysis of accuracy of description of velocities for various empirical functions, a) local verification, b) global verification.

parabola of the second order to approximate the four chosen experimental readings of vertical velocity  $V_y$ . If we do not obtain the zero values of velocities in the assumed approximation then we should apply another function to approximate the experimental values of velocities  $V_y$ . From these two functions we choose the one of the highest value of the coefficient of correlation. The choice of parabolic function for the first approximation came out from the fact that the more there are constant coefficients in the description of the function the more accurate description should be expected. Here we approximated values of velocities by the three proposed types of the functions and we obtained values  $x$  for which  $V_y=0$  (FCB). In symmetric flows the flow channel boundary is defined in a various way. Zhang and Ooi[40] called it as the zone in which the particles do not slough off the solid surface but follow the paths predicted by the kinematic theory all the way to the outlet. The particles located in the surrounding feeding zone enter the top flow layer and roll down to the central axis and then finally move towards the outlet. Many numerous investigations at measuring and predicting the pattern of material flow during silo discharging have been carried out (e.g. Cundall and Strack[16], Nedderman and Tüzün [21]). Tüzün and Nedderman [34] defined the flow channel boundary as the streamline within which 99% of the total flow takes place while Watson and Rotter [36] proposed to define the boundary where the velocity at each level is 1% of the center line velocity at that level. In the case of

**Table 9**  
Values of the flow rate (integrated).

Level H [cm]	$x_n$ [cm]	$Q$ [cm <sup>2</sup> /s]	Sums of the squares of the differences $\sum (Q_{empir} - \bar{Q})^2 \times 10^{-2}$		
			Gaussian description	Description by the ch function	Joined functions
5	6	10.19	10.247	10.268	1.7161
10	8	10.349	10.356	10.460	0.0036
20	11	10.962	10.967	10.959	3.5721
30	15	11.901	11.918	12.016	5.9049
40	16	12.829	12.88	12.819	3.2041
50	18	14.45	14.48	14.254	14.0625
60	21	17.366	17.392	17.303	6.7600
$\sum \sum$					35.2233

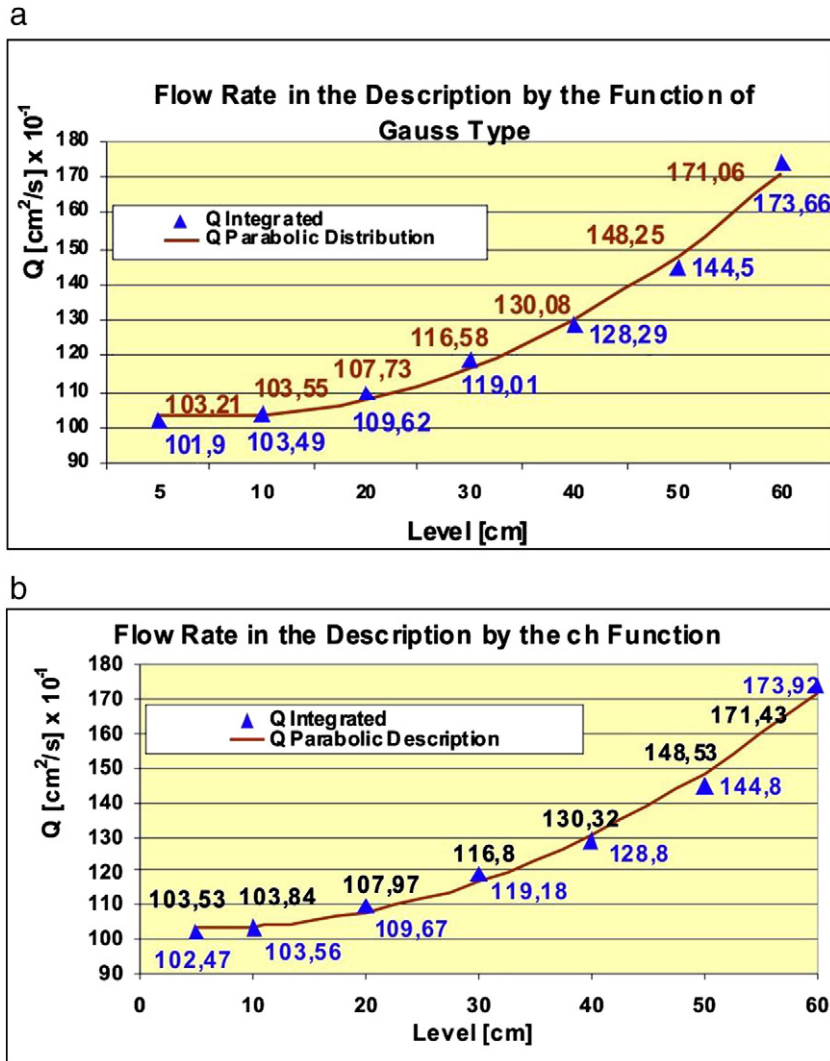


Fig. 12. Comparison of the flow rate calculated by: a) the function of the Gaussian type, b) the *ch* function.

asymmetric flows the maximal velocities occur in various distances from the left wall of the model. Hence the vertical velocity was assumed  $V_y = 0$  at the stagnant zone boundary. The values of  $x$  and the

parameters of the proposed functions are given in Table 14 in Appendix A. On the basis of these data, the points of the calculated values of  $x$  at which vertical velocity  $V_y = 0$  are shown in Fig. 14.

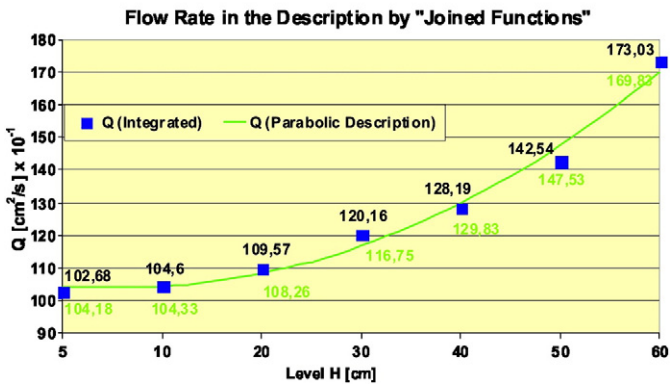


Fig. 13. Flow rate calculated by "the joined functions".

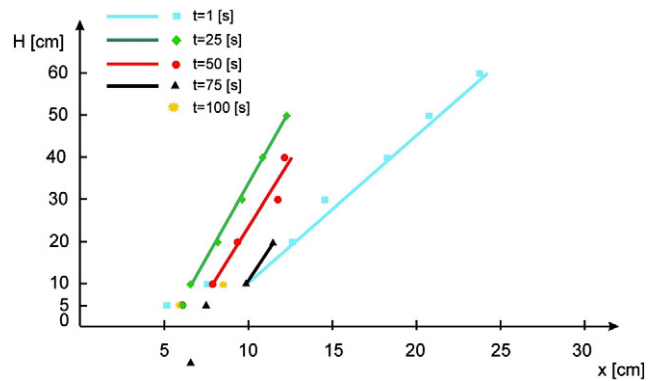


Fig. 14. Range of the stagnant zone boundary at the analyzed instants of the flow.

The regression lines determined on the basis of the data given in Table 14 published in Appendix A are also shown in Fig. 14. The equations of these lines were calculated for the height  $H \geq 10$  cm and they are following:

$$\begin{aligned}
 &\text{–for 1 s of the flow } \hat{x} = 5.923 + 0.306H; \quad r = 0.985 \\
 &\text{–for 25th s of the flow } \hat{x} = 5.335 + 0.1401H; \quad r = 0.999 \\
 &\text{–for 50th s of the flow } \hat{x} = 7.37 + 0.1567H; \quad r = 0.970 \\
 &\text{–for 75th s of the flow } \hat{x} = 8.26 + 0.166H; \quad r = 1
 \end{aligned}
 \tag{15}$$

In the presented analysis we described the distribution of the range of the stagnant zone boundary forming in the flowing material from the level  $H = 10$  cm. For heights  $H \geq 10$  cm it is possible to approximate the stagnant zone boundary by the line. This fact is confirmed by the coefficients of correlation given in Formula (15).

### 5. Conclusions

Methodology of empirical description of vertical velocities in the eccentric filling-discharge process is presented in this paper. The total time of flow for the flax-seed was found to be 123 s. Presented empirical descriptions provided theoretical analysis of choice of proper functions to describe velocities: by the exponential function, modified, the Gaussian type and *ch* function using the 1st, the 2nd and the multiple regression. It was found that the 2nd regression gave the best agreement to the experimental results of the registered velocities. Using the 1st and the multiple regression we obtained almost the same descriptions. The presented way of empirical analysis shows that the given methodology can be applied in describing velocities in any case of eccentric flows in the model of similar parameters i.e. of such height, thickness, with vertical walls, Sielamowicz et al. [30]. Some similar functions were also used in the empirical description of velocities in the converging model for flowing amaranth seeds, Sielamowicz et al. [31]. In Sielamowicz et al. [30], similar functions were applied in the case of eccentric flow – with the outlet located on the right. The authors are preparing a comparative analysis between the results of both and also including the case with the outlet located in the symmetry axis of the model. Both articles mentioned above deal with similar items but the equations used in both are not exactly the same and in the case of the outlet located in the symmetry axis we have some further modifications of the empirical description. Such comparative analysis will show the possibilities how to describe eccentric flows with various locations of the outlet and its influence to the flow parameters. The methodology used appeared very useful to clarify the behavior of the silo discharging phenomena in both kinds of silo models and the proposed descriptions can be applied in empirical analysis for any type of granular materials used in experiments and in models of any geometry of the silo (cf. Sielamowicz et al. [30,31]).

All the data obtained in this paper and in [30] are being used to provide the analysis with the pressures on the silo walls that can be interesting for the researcher in the field.

The values of the flow rate calculated for two empirical descriptions were similar. We can predict the flow rate for the higher levels approximating the given functions in Fig. 8. Because of the complex nature of the flow we presented another description of velocities – by the joined functions. It was found that using the joined function the accuracy of the solution is the best fitted to the experimental results. The solution gives the least sum of the squares of the differences. But it was also stated that

there is no method to describe velocities well fitted to the experimental results both at all analyzed levels and at all measurement points. The empirical description of the joined functions showed that if we can describe velocities due to the lower levels then the description at all measurement points is not too well fitted to the experimental results. Statistical analysis presented in the paper given in Appendix A was made in detail that can be helpful to the readers. Further work is required to describe and predict both the flow channel boundary (FCB) and the flow rate at higher levels in eccentric flows.

### Acknowledgements

The authors express their deep gratitude to Prof. Zenon Mróz of Fundamental Technological Research of Polish Academy of Sciences in Warsaw for all suggestions concerning the analysis of the problem presented in this paper. All experiments in DPIV technique were performed at the Department of Mechanics and Physics of Fluids at the Institute of Fundamental Technological Research of Polish Academy of Sciences in Warsaw. Special thanks directed to Sławomir Błofski, Ph.D for providing numerical results in DPIV technique. The paper was partly prepared under the Rector's Project S/WM/2/08.

### Appendix A

**Table 1**  
Readings at level  $H = 5$  cm.

Time [s]	Velocities [mm/s] at the distance from the symmetry axis $x$ [cm]						
	0	1	2	3	4	5	6
1 s	34.0	33.5	25.0	15.0	4.0	1.0	0
25 s	12.0	20.0	24.0	23.0	15.0	6.0	1.0
50 s	29.5	32.0	31.5	20.0	7.0	5.0	1.0
75 s	25.0	32.5	27.0	15.0	7.0	5.0	3.0
100 s	23.5	27.5	29.0	25.0	13.0	3.0	1.0

**Table 2**  
Readings at level  $H = 10$  cm.

Time [s]	Velocities [mm/s] at the distance from the symmetry axis $x$ [cm]								
	0	1	2	3	4	5	6	7	8
1 s	16.0	16.7	16.0	16.0	12.0	7.0	4.0	1.0	0
25 s	16.5	19.0	20.0	18.5	19.0	15.0	7.0	0	0
50 s	15.0	18.0	19.0	17.0	17.0	16.0	11.0	6.0	0
75 s	13.5	18.0	18.5	18.0	14.0	10.0	8.0	8.0	5.0
100 s	14.0	20.5	21.5	20.0	17.0	12.0	8.0	3.0	1.5

**Table 3**  
Readings at level  $H = 20$  cm.

Time [s]	Velocities [mm/s] at the distance from the symmetry axis $x$ [cm]											
	0	1	2	3	4	5	6	7	8	9	10	11
1	10.0	10.0	11.0	11.5	12.0	11.0	10.0	8.0	6.5	4.0	2.5	2.0
25	12.0	14.5	14.5	14.75	14.5	14.5	13.0	10.0	2.0	0	0	0
50	13.75	14.0	14.75	14.0	13.5	13.0	13.0	12.0	10.0	3.0	0	0
75	12.0	13.5	14.0	13.5	13.5	13.5	12.0	11.0	9.0	5.0	0	0

**Table 4**  
Readings at level H = 30 cm.

Time [s]	Velocities [mm/s] at the distance from the symmetry axis $x$ [cm]															
	0	1	2	3	4	5	6	7	8	9	10	11	12	13	14	15
1	10.0	10.0	10.0	11.0	12.0	11.0	11.0	10.0	9.0	8.0	5.0	4.0	2.5	2.5	2.0	1.5
25	12.0	12.0	12.0	12.5	12.0	12.0	11.5	12.0	10.0	5.0	0	0	0	0	0	0
50	12.5	13.0	13.0	13.0	12.5	12.5	13.3	12.0	10.0	7.0	3.0	3.0	0	0	0	0

**Table 5**  
Readings at level H = 40 cm.

Time [s]	Velocities [mm/s] at the distance from the symmetry axis $x$ [cm]																
	0	1	2	3	4	5	6	7	8	9	10	11	12	13	14	15	16
1	9.5	10.0	10.5	11.0	11.5	11.0	11.0	10.5	10.5	10.0	8.0	7.0	5.0	4.0	2.5	2.0	1.5
25	11.8	11.8	11.8	11.0	11.5	10.5	12.0	11.5	10.0	7.5	4.0	0	0	0	0	0	0
50	11.0	11.5	12.0	12.0	12.0	12.0	11.5	10.5	10.0	9.0	7.0	2.0	0	0	0	0	0

**Table 6**  
Readings at level H = 50 cm.

Time [s]	Velocities [mm/s] at the distance from the symmetry axis $x$ [cm]																		
	0	1	2	3	4	5	6	7	8	9	10	11	12	13	14	15	16	17	18
1	10.0	10.0	10.0	11.0	11.5	10.5	12.5	12.0	12.0	10.0	9.0	8.5	7.5	6.0	5.0	4.0	3.0	2.5	1.5
25	10.	11.0	11.0	10.5	10.5	11.0	11.5	10.0	9.0	8.0	6.5	4.5	1.0	0	0	0	0	0	0

**Table 7**  
Readings at level H = 60 cm.

Time [s]	Velocities [mm/s] at the distance from the symmetry axis $x$ [cm]																					
	0	1	2	3	4	5	6	7	8	9	10	11	12	13	14	15	16	17	18	19	20	21
1	10.0	8.0	11.0	11.5	11.5	12.0	11.5	11.0	12.5	11.5	10.5	10.0	9.0	8.0	6.0	5.5	5.0	5.0	3.0	3.0	2.0	1.5

**Table 8**  
Statistical values for calculation of the confidence interval for level H = 5 cm.

Statistical values	Distance from the symmetry axis [cm]						
	$x=0$	$x=1$	$x=2$	$x=3$	$x=4$	$x=5$	$x=6$
$\bar{V}_y$	24.8	29.1	27.3	19.6	9.2	4.0	1.5
$S$	7.38	4.994	2.713	4.079	4.118	1.789	0.866
$n$	5	5	5	5	5	5	4
$t_{n-1,1-\frac{\alpha}{2}}$	2.7764	2.7764	2.7764	2.7764	2.7764	2.7764	3.1824
$t_{n-1,1-\frac{\alpha}{2}} \frac{S}{\sqrt{n-1}}$	10.24	6.93	3.77	5.66	5.72	2.48	1.59
$\bar{V}_y - t_{n-1,1-\frac{\alpha}{2}} \frac{S}{\sqrt{n-1}}$	14.56	22.17	23.53	13.94	3.48	1.52	0
$\bar{V}_y + t_{n-1,1-\frac{\alpha}{2}} \frac{S}{\sqrt{n-1}}$	35.04	36.03	31.07	25.26	14.92	6.48	3.09

**Table 9**  
Statistical values for calculation of the confidence interval for level H = 10 cm.

Statistical values	Distance from the symmetry axis [cm]								
	$x=0$	$x=1$	$x=2$	$x=3$	$x=4$	$x=5$	$x=6$	$x=7$	$x=8$
$\bar{V}_y$	15.0	18.44	19.0	17.9	15.8	12.0	7.2	4.5	3.25
$S$	1.14	1.263	1.819	1.356	2.482	3.286	2.315	2.693	1.75
$n$	5	5	5	5	5	5	5	4	2
$t_{n-1,1-\frac{\alpha}{2}}$	2.7764	2.7764	2.7764	2.7764	2.7764	2.7764	2.7764	3.184	12.706
$t_{n-1,1-\frac{\alpha}{2}} \frac{S}{\sqrt{n-1}}$	1.58	1.75	2.52	1.88	3.45	4.56	3.21	4.94	22.23
$\bar{V}_y - t_{n-1,1-\frac{\alpha}{2}} \frac{S}{\sqrt{n-1}}$	13.42	16.69	16.48	16.02	12.35	7.44	3.99	0	0
$\bar{V}_y + t_{n-1,1-\frac{\alpha}{2}} \frac{S}{\sqrt{n-1}}$	16.58	20.19	21.52	19.71	19.25	16.56	10.41	9.45	25.49



**Table 12**  
Statistical values for calculation of the confidence interval for level  $H=40$  cm.

Statistical values	Distance from the symmetry axis [cm]																
	x=0	x=1	x=2	x=3	x=4	x=5	x=6	x=7	x=8	x=9	x=10	x=11	x=12	x=13	x=14	x=15	x=16
$\bar{V}_y$	10.77	10.83	11.43	11.33	11.67	11.17	11.5	10.83	10.17	8.83	6.33	4.5	5.0	4.0	2.5	2.0	1.5
S	0.953	0.624	0.665	0.471	0.236	0.624	0.408	0.471	0.236	1.027	1.700	2.500					
n	3	3	3	3	3	3	3	3	3	3	3	2	1	1	1	1	1
$t_{n-1,1-\frac{\alpha}{2}}$	4.3027	4.3027	4.3027	4.3027	4.3027	4.3027	4.3027	4.3027	4.3027	4.3027	4.3027	12.706					
$t_{n-1,1-\frac{\alpha}{2}} \frac{S}{\sqrt{n-1}}$	2.90	1.90	2.02	1.43	0.72	1.90	1.24	1.43	0.72	3.12	5.17	31.77					
$V_y - t_{n-1,1-\frac{\alpha}{2}} \frac{S}{\sqrt{n-1}}$	7.87	8.93	9.41	9.90	10.95	9.27	10.26	9.40	9.45	5.71	1.16	0					
$V_y + t_{n-1,1-\frac{\alpha}{2}} \frac{S}{\sqrt{n-1}}$	11.67	12.73	13.45	12.76	12.39	13.07	12.74	12.26	10.89	11.95	11.50	36.27					

**Table 13**  
Statistical values for calculation of the confidence interval for level  $H=50$  cm.

Statistical values	Distance from the symmetry axis [cm]																			
	x=0	x=1	x=2	x=3	x=4	x=5	x=6	x=7	x=8	x=9	x=10	x=11	x=12	x=13	x=14	x=15	x=16	x=17	x=18	x=19
$\bar{V}_y$	10.25	10.5	10.5	10.75	11.0	10.75	12.0	11.0	10.5	9	7.75	6.5	7.5	6.0	5.0	4.0	3.0	2.5	1.5	0.5
S	0.25	0.5	0.5	0.25	0.5	0.25	0.5	1.0	1.5	1.0	1.25	2.0								
n	2	2	2	2	2	2	2	2	2	2	2	2	1	1	1	1	1	1	1	1
$t_{n-1,1-\frac{\alpha}{2}}$	12.206	12.206	12.206	12.206	12.206	12.206	12.206	12.206	12.206	12.206	12.206	12.206	12.206	12.206	12.206	12.206	12.206	12.206	12.206	12.206
$t_{n-1,1-\frac{\alpha}{2}} \frac{S}{\sqrt{n-1}}$	3.18	6.35	6.35	3.18	6.35	3.18	6.35	12.71	19.06	12.71	15.88	25.41								
$V_y - t_{n-1,1-\frac{\alpha}{2}} \frac{S}{\sqrt{n-1}}$	7.07	4.15	4.15	7.57	4.65	7.57	5.65	0	0	0	0	0								
$V_y + t_{n-1,1-\frac{\alpha}{2}} \frac{S}{\sqrt{n-1}}$	13.43	16.85	16.85	13.93	17.35	13.93	18.35	23.71	29.56	21.71	23.63	31.91								

$\bar{V}_y$  – average vertical velocity.  
 S – standard deviation, Volk [38].  
 $\alpha$  – significance level.  
 n – number of readings.  
 $t_{n-1,1-\frac{\alpha}{2}}$  – quantile of *t*Student distribution.  
 $t_{n-1,1-\frac{\alpha}{2}} \frac{S}{\sqrt{n-1}}$  – half of the confidence interval.  
 $V_y - t_{n-1,1-\frac{\alpha}{2}} \frac{S}{\sqrt{n-1}}$  – lower limit of the confidence interval.  
 $V_y + t_{n-1,1-\frac{\alpha}{2}} \frac{S}{\sqrt{n-1}}$  – upper limit of the confidence interval.



## References

- [1] ACI 313, Alternate design procedure, Discussion Document before ACI Committee 313 on Concrete Bins, Silos and Bunkers for Storing Granular Materials, ACI, Detroit, 1989.
- [2] AS 3774, Loads on Bulk Solids Containers, Australian Standards Association of Australia, Sydney, 1986.
- [3] ENV, Part 4 2002 Eurocode 1, Actions on silos and tanks Brussels, Belgium, , 1991.
- [4] PN-89/B-03262, Polish Standard: Silosy żelbetowe na materiały sypkie. Obliczenia statyczne, , 1989 (in Polish).
- [5] Anon, Reliable flow of particulate solids, EFCE Publication Series (European Federation of Chemical Engineers), 49, 1985.
- [6] F. Ayuga, M. Guaita, P.J. Aguado, A. Couto, Discharge and the eccentricity of the hopper influence on the silo wall pressures, *Journal of Engineering Mechanics* 127 (10) (2001) 1067–1074.
- [7] G.E. Blight, Eccentric discharge of a large coal bin with six outlets, *Bulk Solids Handling* 11 (2) (1991) 451–457.
- [8] A. Borcz, el Rahim Hamdy Abd, Wall pressure measurements in eccentrically discharged cement silos, *Bulk Solids Handling* 11 (2) (1991) 469–476.
- [9] J.W. Carson, Silo failures: case histories and lessons learned, Third Israeli Conference for Conveying and Handling of Particulate Solids, Dead Sea Israel, May 2000.
- [10] J.F. Chen, J.M. Rotter, J.Y. Ooi, Z. Zhong, Flow patterns measurement in a full scale silo containing iron ore, *Chemical Engineering Science* 60 (2005) 3029–3041.
- [11] J. Choi, A. Kudrolli, M.Z. Bazant, Velocity profile of granular flow inside silos and hoppers, *Journal of Physics. Condensed Matter* 17 (2005) S2533–S2548.
- [12] C.S. Chou, J.Y. Hsu, Y.D. Lau, Flow patterns and stresses on the wall in a two-dimensional flat-bottomed bin, *Journal of Chinese Institute of Engineers, Transactions of the Chinese Institute of Engineers, Series A* 26 (4) (2003) 397–408.
- [13] C.S. Chou, Y.C. Chuang, J. Smid, S.S. Hsiau, J.T. Kuo, Flow patterns and stresses on the wall in a moving granular bed with eccentric discharge, *Advanced Powder Technology* 13 (1) (2002) 1–13.
- [14] C.S. Chou, J.Y. Hsu, Kinematic model for granular flow in a two-dimensional flat-bottomed hopper, *Advanced Powder Technology* 14 (3) (2003) 313–331.
- [15] H. de Clercq, Investigation into stability of a silo with concentric and eccentric discharge, *Civil Engineers in South Africa* 32 (3) (1990) 103–107.
- [16] P.A. Cundall, O.D.L. Strack, A discrete numerical model for granular assemblies, *Geotechnique* 29 (1) (1979) 47–65.
- [17] J.S. Guaita, A. Couto, F. Ayuga, Numerical simulation of wall pressure during discharge of granular material from cylindrical silos with eccentric hoppers, *Biosystem Engineering* 85 (1) (2003) 101–109.
- [18] U. Haussler, J. Eibl, Numerical investigations on discharging silos, *Journal of Engineering Mechanics, Division ASCE* 110 (1984) 957–971 EM6.
- [19] A.W. Jenike, Denting of circular bins with eccentric draw points, *Journal of the Structural Division ASCE* 93 (1967) 27–35 (ST1).
- [20] M. Molenda, J. Horabik, S.A. Thompson, I.J. Ross, Bin loads induced by eccentric filling and discharge of grain, *Transactions of the ASAE* 45 (3) (2002) 781–785.
- [21] R.M. Nedderman, U. Tüzün, A kinematic model for the flow of granular materials, *Powder Technology* 22 (1979) 243–253.
- [22] D.K. Pokrant, M.G. Britton, Investigation into the effects of eccentric draw off and flow rate in model grain bin studies, *Paper-American Society of Agricultural Engineers* (1986) 86–4076.
- [23] G.M. Quenot, J. Pakleza, T.A. Kowalewski, Particle image velocimetry with optical flow, *Experiments in Fluids* 25 (1998) 177–189.
- [24] J.M. Rotter, The analysis of steel bins subject to eccentric discharge, *Proc., 2nd Inter. Conference on Bulk Materials Storage Handling and Transportation, Ins. of Eng., Wollongong, Australia, July 1986*, pp. 264–271.
- [25] J.M. Rotter, J.Y. Ooi, C. Lauder, I. Coker, J.F. Chen, B.G. Dale, A study of the flow patterns in an industrial silo, *Proceedings RELPOWFLO II, Oslo, August 1993*, pp. 517–524.
- [26] J.M. Rotter, *Guide for the Economic Design of Metal Silos*, E&FN Spon, London, 1998.
- [27] K. Runesson, L. Nilsson, Finite element modelling of the gravitational flow of a granular material, *Bulk Solids Handling* 6 (5) (1986) 877–884.
- [28] S.S. Safarian, E.C. Harris, Post-tensioned circular silos for modern industry, *Bulk Solids Handling* 7 (1987) 2.
- [29] F. Shalouf, S. Kobiellak, Reduction of the dynamic flow pressure in grain silo by using discharge tubes, *Powder Handling Processing* 13 (2001) 1.
- [30] I. Sielamowicz, M. Czech, T.A. Kowalewski, Empirical description of flow parameters in eccentric flow inside a silo model, *Powder Technology* 198 (2010) 381–394.
- [31] I. Sielamowicz, M. Czech, Investigation of the radial flow assumption in a converging model silo, *Biosystems Engineering* 106 (4) (2010) 412–422.
- [32] C.Y. Song, J.G. Teng, Buckling of circular steel silos subject to code-specified eccentric discharge pressures, *Engineering Structures* 25 (2003) 1397–1417.
- [33] S.A. Thompson, J.L. Usry, J.A. Legg, Loads in a model grain bin as affected by various unloading techniques, *Transactions of the ASAE* 29 (1986) 2.
- [34] U. Tüzün, R.M. Nedderman, Experimental evidence supporting kinematic modelling of the flow of granular media in the absence of air drag, *Powder Technology* 24 (1979) 257–266.
- [35] U. Tüzün, R.M. Nedderman, An investigation of the flow boundary during steady-state discharge from a funnel flow bunker, *Powder Technology* 31 (1) (1982) 27–43.
- [36] G.R. Watson, J.M. Rotter, A finite element kinematic analysis of planar granular solids flow, *Chemical Engineering Science* 51 (16) (1996) 3967–3978.
- [37] W. Volk, *Applied Statistics for Engineers*, second edition Mc Graw-Hill, 1969.
- [38] M. Wójcik, G.G. Enstad, M. Jecmenica, Numerical calculations of wall pressures and stresses in steel cylindrical silos with concentric and eccentric hoppers, *Journal of Particulate Science and Technology* 21 (3) (2003) 247–258.
- [39] J.G.M. Wood, The analysis of silo structures subject to eccentric discharge, *Proc., 2nd Int. Conf. on Design of Silos for Strength and Flow, Stratford-upon-Avon, 1983*, pp. 132–144.
- [40] K.F. Zhang, J.Y. Ooi, A kinematic model for solids flow in flat bottomed silos, *Geotechnique* 48 (4) (1998) 545–553.